Composites: Part A 179 (2024) 108040

Contents lists available at ScienceDirect

Composites Part A

journal homepage: www.elsevier.com/locate/compositesa

A state-rate model for the transient wall slip effects in ply-ply friction of UD C/PAEK tapes in melt

E.R. Pierik [a,b], W.J.B. Grouve [a,*], S. Wijskamp [b], R. Akkerman [a,b]

[a] Faculty of Engineering Technology, Chair of Production Technology, University of Twente, Drienerlolaan 5, Enschede, 7522 NB, The Netherlands
[b] ThermoPlastic composites Research Center (TPRC), Palatijn 15, Enschede, 7521 PN, The Netherlands

ARTICLE INFO

Dataset link: 4TU.ResearchData

Keywords:
A. polymer-matrix composites (PMCs)
A. thermoplastic resin
B. rheological properties
E. forming
Friction

ABSTRACT

Ply-ply slippage is one of the key deformation mechanisms occurring during hot press-forming of thermoplastic composite laminates. Advanced forming simulations, required for defect-free manufacturing, rely on accurate constitutive models for these deformation mechanisms. In this work, we propose a relative simple, yet accurate, transient model to describe the start-up friction response of UD C/PAEK tapes. The model combines a White–Metzner viscoelastic fluid with a state-rate model for the evolution of wall slip near the fiber–matrix interface, describing the disentanglement of surface polymer chains followed by the settlement of these chains in a new equilibrium state. This allows prediction of the stress growth at start-up and the transition from peak to steady-state friction, from smooth to sharp with increasing sliding rate, as well as the magnitude of the peak and steady-state friction. We obtained a good correlation between the modeled and measured friction response for different sliding rates.

1. Introduction

Continuous fiber reinforced thermoplastics allow for rapid, cost-efficient manufacturing of small to medium-sized parts by means of hot press forming. Over the years, simulation software for press forming proved its value for industry by reducing trial-and-error costs involved with the development of new thermoplastic matrix composite (TPC) parts. However, more accurate predictions, particularly for defect generation, are needed to further facilitate the design stage. In turn, this requires accurate material characterization and constitutive modeling.

The deformation behavior of a composite laminate during forming is classified in several mechanisms, of which intra-ply shear, inter-ply slippage and ply bending are recognized as the most important ones [1,2]. These deformation mechanisms are separately quantified in characterization experiments, modeled, and, subsequently, combined in a numerical solver to describe the deformation of the material. The numerical code allows the simulation of the hot press forming of TPCs and enables virtual design iterations. This work focuses on one of the important deformation mechanisms, namely ply-ply slippage, to follow-up on our earlier work [3–5]. Ply-ply slippage is required to form defect-free parts, as it allows for intra-ply shear and bending of the laminate [6–8]. Recent work on intra-ply shear and bending can be found in e.g. Refs. [9–11].

The typical friction response of a molten TPC, as measured in a characterization experiment where a central ply is forced to slide against plies at each side [2,12–16], is shown in Fig. 1. A peak shear stress τ_p emerges at higher rates, followed by a stationary regime marked by a steady-state or long-time shear stress τ_∞. For low sliding rates, no peak appears as the shear stress increases monotonically towards a steady-state. The long-time shear stress is often considered in modeling, following the hydrodynamic lubrication regime of the Stribeck curve for woven reinforcements [6,17,18] or by means of a description that includes a yield stress or Coulomb friction superimposed with a viscous term [2,12,16,19]. Earlier research has shown that the hydrodynamic lubrication approach fails to describe the friction of unidirectional (UD) C/PEEK tapes [2,20].

Recently, we proposed a slip relaxation effect, resulting in a gradual increase in slip between fiber and matrix, as the most probable explanation for the transient ply-ply friction response [3], in line with earlier work [2]. These insights were used to develop a model based on shear flow of the matrix material at the ply-ply interface to predict the peak shear stress τ_p [4]. Additionally, we included a critical shear stress to represent the effect of wall slip, following the findings on pure polymers [21–24], to successfully predict the long-time shear stress τ_∞ as well. This framework was extended in later work to include the effect of temperature and normal pressure [5].

Although the proposed shear flow model accurately describes the peak and long-time shear stress and adds to our understanding of

* Corresponding author.
E-mail address: w.j.b.grouve@utwente.nl (W.J.B. Grouve).

https://doi.org/10.1016/j.compositesa.2024.108040
Received 9 October 2023; Received in revised form 4 January 2024; Accepted 19 January 2024
Available online 29 January 2024
1359-835X/

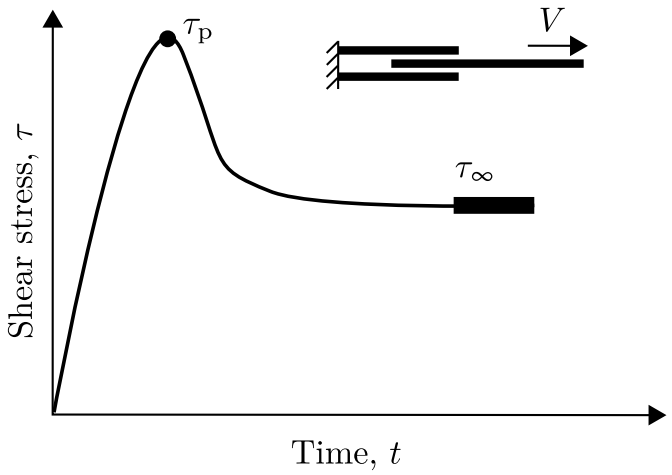

Fig. 1. Schematic friction response showing start-up behavior with time as typically observed in characterization experiments on molten TPCs [4].

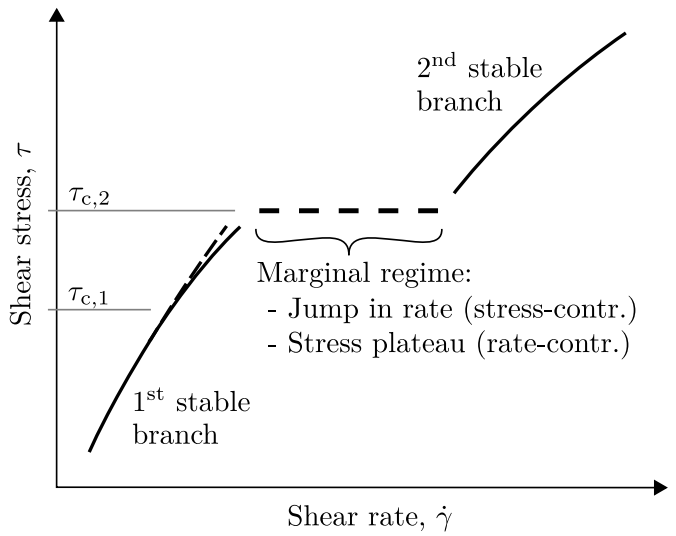

Fig. 2. Schematic flow curve of the stationary shear stress vs. shear rate as observed for different polymer melts in literature (e.g. polyethylenes, polybutadienes, polystyrenes, polyisoprenes, polydimethylsiloxanes, fluoropolymers), visualizing a first and second stable branch with a marginal regime in between. This marginal regime results in a shear rate jump (spurt) in case of stress-controlled experiments, while a shear-stress plateau emerges in case of rate-controlled experiments.
Source: Illustration based on Refs. [21–24,31,34,35].

the underlying mechanism for ply-ply friction, the model still lacks a description of the full transient response, including stress growth at start-up and the transition from τ_p to τ_∞. Some studies addressed the modeling of the full friction response, without consideration of the underlying physics, and employed a linear [7] or exponential decay [25] to describe the τ_p-to-τ_∞-transition or used a cohesive zone model originating from crack simulations in fracture mechanics [26]. The latter approach was also used by Kapshammer et al. [27] more recently.

In this paper, we extend our earlier shear flow model [4] to describe the full transient friction response for different constant sliding rates. A proper description of the transient response will improve the predictive quality of the forming simulations, especially if we consider that the relative small ply-ply slippage encountered in practice often corresponds to the transient region of the characterization experiment [2,16]. The transient model proposed here is based on a gradual increase of wall slip near the fiber–matrix interface, which is caused by the disentanglement of polymer chains adsorbed to the fiber from the bulk polymer chains upon shearing. This process of disentanglement is described using a state-rate model, which is related to the local slip velocity. The resulting evolution of the slip velocity is then combined with a White–Metzner viscoelastic fluid [28]. The transient shear flow model accurately describes the measured friction curves of UD C/PEEK and C/LM-PAEK for different sliding rates.

2. Background

Our combined experimental and modeling work presented earlier [3–5] revealed a slip relaxation effect as the underlying mechanism for the ply-ply friction. These insights were based on a strong resemblance of our experimental observations with findings on shear flow of pure polymers, which form the basis for the modeling work in this research. A brief background on the observations with pure polymers will be presented first, followed by relevant models.

2.1. Wall slip

Hatzikiriakos and co-workers [21,29,30] and others [24,31] performed experiments on pure polymer melts using a rate-controlled sliding plate rheometer to investigate the effect of wall slip on the shear stress response. They reported a dependency of the stationary shear stress on the gap height due to a nonzero velocity near the polymer-wall interface [29,30]. Furthermore, at high rates, the stationary values were limited to a certain critical shear stress, resulting in a shear-stress plateau in a flow curve of shear stress versus the applied rate [24,31]. A schematic flow curve as observed for different polymer melts is visualized in Fig. 2, where the dashed horizontal line (marginal regime) represents the shear-stress plateau. Similarly, Boukany et al. [23] found a jump in the shear rate at the critical shear stress in stress-controlled sliding plate rheometry tests, visualized in Fig. 2 by the discontinuity between the first and second stable branch, which relates to the observations of a spurt flow in polymer extrusion or capillary rheometry [21–23]. Techniques such as particle tracking velocimetry were used to visualize the velocity profile upon shearing or extrusion, proving the existence of a nonzero slip velocity near the wall [22,32,33].

The slip velocity near the wall could originate from two mechanisms, namely the desorption of polymer chains from the wall or the disentanglement of adsorbed polymer chains from the bulk ones [21–23,32,34,36]. The presence and severity of the two slip regimes depends, among others, on the degree of polymer chain adsorption. In general, the former is commonly labeled as weak slip, which emerges from a first critical shear stress $\tau_{c,1}$ and often results in only small deviations from the no-slip condition as visualized by the dashed line in Fig. 2. The latter mechanism is labeled as strong slip, leading to large slip velocities and the mentioned discontinuity in the flow curve occurring at a second critical shear stress $\tau_{c,2}$. Dating back to the 70s, Bergem [37] was one of the first to propose this disentanglement of surface polymer chains from the bulk as the underlying mechanism for the discontinuity during extrusion of HDPE melts. In our earlier work [4], we considered the effect of strong slip at the fiber–matrix interface by limiting the viscous shear stress in the matrix interlayer to $\tau_{c,2}$. Using this approach, we obtained an accurate prediction of the measured long-time shear stress as function of the applied sliding rate.

The term slip relaxation effect was used to denote the evolution of the slip velocity from zero to the steady-state value in transient wall slip experiments [21,30]. Hence, shear stress peaks, higher than $\tau_{c,2}$, were observed in start-up shear flow experiments at high rates before a steady-state shear stress was attained [36,38]. This time-dependency relates to the time required for the disentanglement of surface chains from the bulk, meaning that the shear stress at start-up shear is not yet or only slightly affected by wall slip. We used this (approximate)

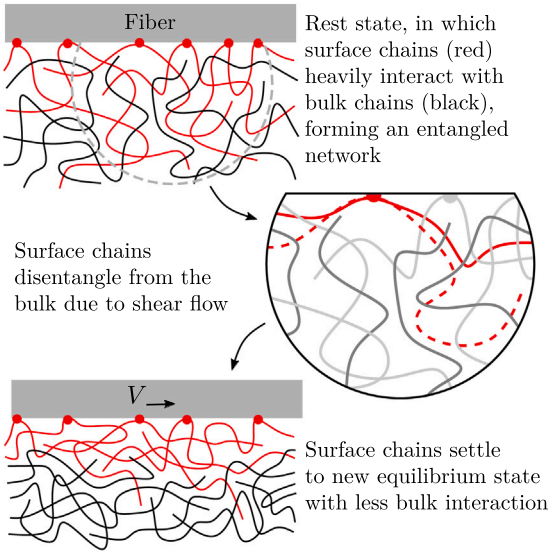

Fig. 3. Schematic illustration of the concept of disentanglement as considered in this study based on the theory of Brochard and de Gennes [35].

no-slip condition in our earlier work [4] to predict the measured peak friction. Now, the evolution of the slip velocity needs to be included in the model, for which the disentanglement of surface chains will be discussed next.

2.2. Polymer chain disentanglement

The scaling theory of Brochard and de Gennes [35], further refined in later work [39], provides a basis for the disentanglement process as discussed in flow of pure polymers [22,33,34,36]. These authors considered a polymer melt with surface chains tethered to a wall. At rest, the polymer chains are entangled and, therefore, form a temporal network. Upon shearing, a tethered chain deforms due to frictional and elastic forces. At a critical rate, the surface chain undergoes a coil-to-stretch transition and disentangles from the bulk. Consequently, the friction reduces and the disentangled chain relaxes. The recoiled chain could, subsequently, re-entangle with the bulk chains, increasing the friction again, leading to the coil-to-stretch transition and so on. Hence, a so-called marginal regime for a range of applied rates emerges, as visualized by the dashed horizontal line in Fig. 2 [35,39]. This marginal regime, characterized by a constant shear stress, was experimentally verified using rate-controlled experiments by e.g. [24,31] and explains the jump in shear rate at $\tau_{c,2}$ as observed with stress-controlled experiments [21–23]. At even higher rates, re-entanglement becomes unfavorable and the surface chains form a fully disentangled layer. A comparable view on flow-induced disentanglement was given in other works [22,33,40], mentioning the elastic build up to a point at which mutual chain sliding occurs between surface and bulk chains due to a "molecular force imbalance", sometimes labeled as yielding [22,33]. A schematic illustration of the process of disentanglement upon shearing as considered in this work is shown in Fig. 3. All in all, the disentanglement of surface chains from the bulk leads to an apparent slip velocity through a reduced interfacial viscosity and, therefore, results in a lower shear stress than expected from the bulk viscosity [22,41].

2.3. Transient wall slip modeling

The slip relaxation can be modeled directly through prescribing the slip velocity based on measured data, a phenomenological approach, or indirectly by considering the underlying polymer dynamics, a first principles approach. Modeling efforts based on both approaches will be discussed briefly in this section.

2.3.1. Phenomenological approaches

Hatzikiriakos and Dealy [29] proposed a phenomenological approach for the evolution of the slip velocity by means of a differential equation, resembling the Maxwell equation for viscoelasticity (VE) with a certain slip relaxation time. A power law was used to describe the stationary slip velocity as a function of the shear stress. Ebrahimi et al. [42] combined this differential equation with a VE model to successfully describe the start-up shear stress for entangled polymer melts. Multiple slip relaxation times were considered in other studies to improve the correlation between model and measurement [30,43]. Similar equations were used to obtain analytical solutions for the shear flow of Newtonian fluids with slip relaxation [44] or to describe the slip extrapolation length [45].

The use of a power law to describe the stationary slip velocity as a function of the shear stress precludes modeling within the marginal regime. This limitation is not important in view of polymer extrusion, as the shear rate simply jumps between the first and the second branch in the flow curve (see Fig. 2). The corresponding jump in the slip velocity was modeled by Hatzikiriakos and Dealy [46] using a discrete transition between two power law relations. In contrast, a description of the slip velocity within the marginal regime is of interest for the current study, in which the rate-controlled friction tests avoid a shear rate jump and, therefore, allows for a shear stress response within the marginal regime.

2.3.2. First principles approaches

The disentanglement of surface and bulk chains, as illustrated in Fig. 3, could be used to model the effect of wall slip instead of directly describing the slip velocity as outlined above. For example, transient network models were employed [47,48], in which entanglements break and form continuously to reflect the polymer interactions near the wall, resulting in a qualitative description of the start-up response. Subsequently, more sophisticated models were proposed [49–51], considering arm retraction and (convective) constraint release as possible relaxation mechanisms for the surface chains. These models described the marginal regime of the stationary slip velocity, though they were not used to describe the start-up response. Kirk et al. [52] showed in a molecular dynamics simulation the coil-to-stretch transition of surface polymer chains as described by Brochard and de Gennes [35], but the computational effort is large.

A more straightforward approach was proposed by Black and Graham [53], who used a structure parameter in a differential equation to describe the entanglement density of surface and bulk chains, relating to the earlier mentioned transient network models and the slip evolution equation of Hatzikiriakos and Dealy [29]. Creation and destruction of the entanglements were based on the number of free and bonded segments. Lan et al. [54] adjusted this model to describe the weak slip regime in start-up exponential shear, as the adsorption and desorption of surface chains resemble a creation and destruction process. Although the current research deals with strong slip and a constant sliding rate, the modeling approach is of interest here due to its relative simplicity and physical considerations. Joshi et al. [55] illustrated the process of disentanglement further by considering kinetic reactions between entangled and disentangled surface chains with empirical rate functions that describe the entanglement–disentanglement dynamics, based on the work of Ahn and Osaki [56]. A similar approach was pursued by Lau and Schowalter [57], who considered activated rate processes for conversions between free and bonded chains.

Application of the mentioned models to the current problem is not straightforward and we found that the given descriptions for the slip evolution, both the phenomenological and the first principles approach, were insufficient to describe the measured ply-ply friction response. Hence, our modeling effort to obtain an accurate description for the friction response will be presented next.

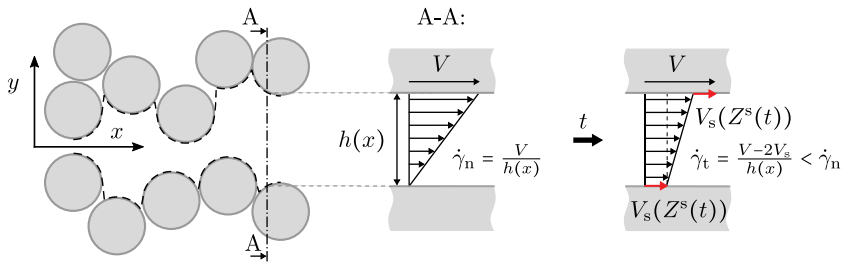

Fig. 4. Schematic illustration of a ply-ply cross section with fibers (gray circles) from a top and bottom ply with a matrix interlayer in between (dashed lines along the relevant fiber edges). Relative motion between the plies generates a nominal shear rate distribution $\dot{\gamma}_n(x)$ in the matrix interlayer, as illustrated in the A-A side view for a matrix interlayer thickness $h(x)$. A slip velocity V_s near the fiber–matrix interface reduces the bulk deformation to a true shear rate $\dot{\gamma}_t$. The time-dependency of V_s is considered in this work through the steady state $Z^s(t)$ of the polymer chains near the fiber–matrix interface as explained in Section 3.3.
Source: Illustration adapted from [4].

3. Modeling work

Our goal is to accurately describe the macroscopic ply-ply friction response as visualized in Fig. 1, without having to deal with computationally expensive models as we have to keep in mind the intended implementation in forming simulation software. Hence, we propose a state-rate model as a simple yet accurate approach, based on the underlying mechanisms as outlined (see Fig. 3), to model the evolution of the slip velocity. This evolution will be used to change the boundary condition in a White–Metzner viscoelastic fluid [28]. Our earlier shear flow model [4] will form the starting point.

3.1. Shear flow model

In our earlier model, we considered the matrix material at the ply-ply interface to be subjected to shear flow with a no-slip and slip condition to predict the measured peak τ_p and long-time shear stress τ_∞, respectively. A schematic illustration of a ply-ply cross-section is shown in Fig. 4, with fibers of adjacent plies separated by the x-axis and surrounded by the molten matrix. The thickness of the matrix interlayer changes over the width of the ply-ply interface, as indicated in the illustration by the dashed black line along the relevant fiber edges, resulting in a matrix interlayer thickness distribution $h(x)$. We obtained $h(x)$ from cross-sectional micrographs of tested specimens as well as from generated fiber distributions [4]. Applying a sliding rate V on the top ply in the fiber direction generates a shear rate in the matrix interlayer, which is visualized in the side views on the right part of Fig. 4. A nominal shear rate distribution $\dot{\gamma}_n(x)$ appears equal to V divided by $h(x)$, which combined with the viscosity of the matrix material leads to a viscous shear stress distribution $\tau_{visc}(x)$ at the ply-ply interface. Strong wall slip was implemented through a second critical shear stress $\tau_{c,2}$, locally representing the effect of fully-developed wall slip in the marginal regime. Consequently, a slip velocity V_s emerges, which reduces the deformation experienced by the bulk material to a true shear rate $\dot{\gamma}_t$:

$$\dot{\gamma}_t(x) = \frac{V - 2V_s}{h(x)}. \tag{1}$$

The lower shear rate due to the slip condition reduces the shear stress distribution to $\tau_{slip}(x)$. Subsequently, the shear stress distributions can be integrated over the width w of the ply-ply interface:

$$\tau_{avg} = \frac{1}{w}\int_0^w \tau(x)\,\mathrm{d}x, \tag{2}$$

to yield an average shear stress for the no-slip and slip condition, which were used in our earlier work to predict τ_p and τ_∞, respectively, as function of the applied sliding rate [4]. Note that this approach is limited to sliding rates up to the end of the marginal regime, as the predicted τ_∞ is bounded by $\tau_{c,2}$. It is expected that τ_∞ exceeds $\tau_{c,2}$ for rates beyond the marginal regime, following a second stable branch as visualized in Fig. 2. The end of the marginal regime, however, was not observed in our earlier experimental work [4,5].

This shear flow model lacks a description for the transition between τ_p and τ_∞, as the considered V_s is time-independent and either zero or equal to the fully-developed slip velocity. In the current work, we propose to include the evolution of V_s.

3.2. Constitutive behavior

A viscoelastic constitutive model is required to describe the behavior of the matrix material. The viscous part of this model should align with our shear flow model, in which we included shear thinning of the matrix material. The White–Metzner model can be used to describe the non-Newtonian behavior [28,58]:

$$\boldsymbol{\tau} + \lambda(\dot{\gamma}_t)^{\triangledown} = 2\eta(\dot{\gamma}_t)\boldsymbol{D} \quad \text{with} \quad \lambda(\dot{\gamma}_t) = \frac{\eta(\dot{\gamma}_t)}{G}, \tag{3}$$

with λ the relaxation time, η the matrix viscosity, G the stiffness, $\boldsymbol{\tau}$ the stress tensor, and $\boldsymbol{D}$ the rate of deformation tensor. In case of a 1D homogeneous shear flow, the White–Metzner model reduces to [19,59]:

$$\tau_{12} + \lambda(\dot{\gamma}_t)\frac{\mathrm{d}\tau_{12}}{\mathrm{d}t} = \eta(\dot{\gamma}_t)\dot{\gamma}_t, \tag{4}$$

with $\dot{\gamma}_t$ the true shear rate (Eq. (1)) and τ_{12} the local viscoelastic shear stress for a certain matrix interlayer thickness in $h(x)$, of which the average can be computed using Eq. (2). A Runge–Kutta time integration scheme was used to solve the differential equation with a sufficiently small time step of 0.01 s.

Apart from a viscoelastic contribution to the ply-ply friction, a contribution from a yield stress τ_y needs to be considered. This yield stress was obtained from the residual stress measured after cessation of the sliding movement in ply-ply friction tests [4]. The findings of Murtagh et al. [12] on ply-ply friction of C/PEEK suggest that this yield stress remains constant throughout the test, and is attributed to fiber–fiber contact [19,60,61]. Hence, the average measured τ_y from our earlier work [4], around 1.8 and 0.5 kPa for C/PEEK at 385 °C and C/LM-PAEK at 365 °C, respectively, needs to be added to the averaged viscoelastic response from Eqs. (4) and (2) to obtain the total shear stress:

$$\tau = \tau_{12,avg} + \tau_y, \tag{5}$$

which can then be compared with the measured ply-ply friction response.

3.3. Changing boundary condition: evolution of the slip velocity

The evolution of the local slip velocity at the fiber–matrix interface is needed to describe the slip relaxation effect. In this section, we will propose a state-rate model for the disentanglement process to describe the evolution of the slip velocity V_s, resembling the approaches of Refs. [47,55].

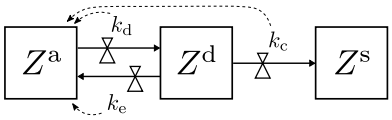

Fig. 5. The proposed state-rate model to describe the average dynamics of the surface polymer chains, starting from an initially entangled network (active state Z^a equals unity). Upon sufficient shearing, surface chains start to disentangle (Z^d with rate k_d) and either re-entangle (rate k_e) or conform themselves to the applied shear flow by settling in the steady state (Z^s, with conformation rate k_c) leading to less bulk interaction.

Following the schematic illustration of Fig. 3, we consider a state-rate model with three states for the surface polymer chains adsorbed to the fiber surface (shown in red): an active Z^a, disentangled Z^d, and steady Z^s state. The states Z^i are an average representation of the surface chains with rates k_i between them, reflecting the polymer dynamics. A schematic illustration of the proposed state-rate model is shown in Fig. 5. In rest, the surface chains heavily interact with the bulk chains through entanglements and, therefore, the active state Z^a equals unity before the shear deformation starts. If the local shear stress due to the applied shear deformation reaches $\tau_{c,2}$, wall slip starts to occur through disentanglement. The entangled surface chains become tensioned and consequently deformed, leading to retraction from the bulk. The average disentanglement of surface chains is modeled through a flow from Z^a to the disentangled state Z^d with disentanglement rate k_d. Once retracted, disentangled surface chains relax and could re-entangle, resulting in a backflow from Z^d to Z^a with entanglement rate k_e, or surface chains could settle into a new equilibrium, conforming to the applied shear deformation, described by a flow to the steady state Z^s with conformation rate k_c. Note that Z^s does not necessarily reflect a fully-disentangled state, as interaction with the bulk chains is still likely to occur albeit on a lower scale. The underlying set of differential equations read:

$$\begin{aligned}\frac{dZ^a}{dt} &= -k_d Z^a + k_e Z^d,\\ \frac{dZ^d}{dt} &= k_d Z^a - k_e Z^d - k_c Z^d,\\ \frac{dZ^s}{dt} &= k_c Z^d \quad \text{with} \quad 0 \le Z^i \le 1.\end{aligned} \tag{6}$$

Next, the three rates k_i connecting the states need to be addressed. As indicated by the dashed arrow in Fig. 5, we propose that the disentanglement rate k_d depends on the active state Z^a. Namely, surface chains will be less likely to disentangle when a lot of neighboring chains still heavily interact with the bulk chains, while with more chains settled in the steady state, the more likely it becomes that active surface chains retract as well as they will experience larger stresses. Hence, as a first step, we used a linear interpolation between a minimum rate k_{min} and a maximum rate k_{max}, depending on Z^a. We expect the opposite effect to happen with the re-entanglement of surface chains, as this re-entanglement will be hindered with an increasing slip velocity through less interactions between surface and bulk chains, while enhancing the settlement into the steady state Z^s. Therefore, the entanglement rate k_e decreases from k_{max} to k_{min} with decreasing Z^a. As a first step, we set the conformation rate k_c equal to k_d following the same reasoning. In the end, we have the following formulations for the rates:

$$\begin{aligned}k_d &= k_{min} Z^a + k_{max}(1 - Z^a),\\ k_e &= k_{max} Z^a + k_{min}(1 - Z^a),\\ k_c &= k_d.\end{aligned} \tag{7}$$

A Forward Euler time integration was used to solve the differential equations (Eq. (6)) with the same, sufficiently small, time step of 0.01 s as used for Eq. (4). A typical evolution of the states is visualized in Fig. 6, illustrating the decrease in the active state Z^a while the surface chains settle in the steady state Z^s smoothly from zero to unity.

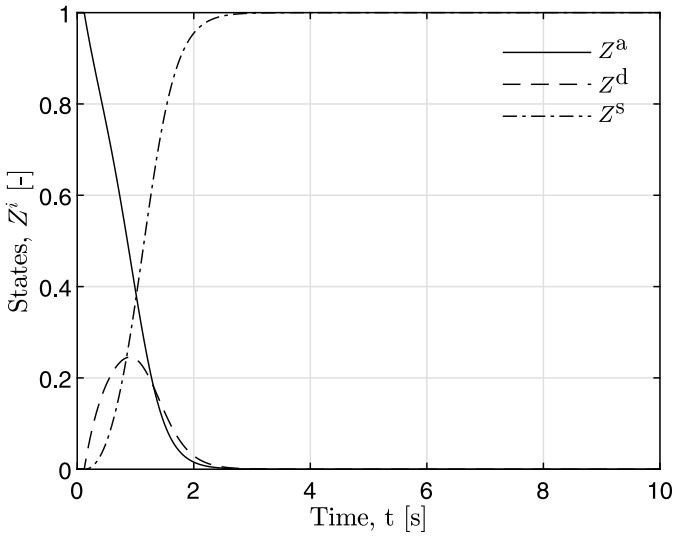

Fig. 6. Evolution of the average state of the surface chains using model parameters for C/PEEK as obtained later in this study (see Table 1) with a sliding rate V of 60 mm/min and a certain matrix interlayer thickness h of 1.5 μm.

This evolution depends on the sliding rate and the local matrix interlayer thickness, which varies along the width of the ply-ply interface. Consequently, the local evolution varies along the width as well.

The proposed evolution of the average state of the surface chains was subsequently used to describe the slip relaxation effect, characterized by a gradual increase of the (apparent) slip velocity V_s. That is, the settlement of surface chains in the steady state ($Z^s \to 1$) reduces the interaction between surface and bulk chains and, therefore, reflects the gradual increase of wall slip. Hence, we propose a direct relation between Z^s and the slip velocity:

$$V_s(t) = V_{s,\infty} Z^s(t), \tag{8}$$

which is used to reduce the nominal shear rate $\dot{\gamma}_n$ to the true shear rate $\dot{\gamma}_t$, according to Eq. (1), consequently reducing the shear stress in the White–Metzner model (Eq. (4)). The fully-developed slip velocity $V_{s,\infty}$ can be obtained by equating the local slip-corrected viscous shear stress with the stress state near the fiber–matrix interface in steady-state, i.e. $\tau_{c,2}$. Thus, the White–Metzner differential equation (Eq. (4)) in steady-state:

$$\tau_{c,2} = \eta(\dot{\gamma}_t)\dot{\gamma}_t, \tag{9}$$

needs to be solved for $\dot{\gamma}_t$, from which $V_{s,\infty}$ can be obtained by using Eq. (1).

Lastly, we considered an effect of the applied sliding rate V on the rates k_i, such that the process of disentanglement occurs at a faster pace with increasing V. We propose a power law relation for the maximum rate k_{max}:

$$k_{max} = k_{min} + aV^m, \tag{10}$$

leading to three fit parameters to describe the slip evolution: k_{min}, a, and m.

3.4. Parameter determination

A part of the parameters required for the proposed transient model were adopted from our earlier work [4]. The second critical shear stress $\tau_{c,2}$, a material parameter, was set equal to the earlier experimentally determined values, namely 35 and 55 kPa for C/PEEK and C/LM-PAEK, respectively. The model requires a matrix interlayer thickness distribution $h(x)$, which can be obtained from cross-sectional micrographs of tested specimens. In our earlier work [4], we showed that

Table 1
Overview of the used variables and parameters for C/PEEK and C/LM-PAEK friction modeling. Fit parameters were manually determined as explained in Section 3.4.

	C/PEEK	C/LM-PAEK	Comment
$h(x)$	–	–	Single matrix interlayer thickness distribution determined from generated fiber distribution [4], see Fig. 12(a).
$\eta(\dot{\gamma})$	–	–	Cross model fit for each material, see Fig. 7.
$\tau_{c,2}$	35 kPa	55 kPa	Critical shear stress derived from measurement [4].
τ_y	1.8 kPa	0.5 kPa	Yield stress derived from measurement [4].
G	500 Pa	400 Pa	Stiffness parameter fit to measured slope during start-up.
k_{min}	0.75	1.8	Slip parameter fit to response at low sliding rates by imposing $k_{max} = k_{min}$.
a	4.6	0.25	Slip parameter for sliding rate dependency based on fit of k_{max} at higher rates according to Eq. (10).
m	1.95	4.2	Slip parameter for sliding rate dependency based on fit of k_{max} at higher rates according to Eq. (10).

mimicking the ply-ply interface through generated fiber distributions yields a similar response. We generated ten matrix interlayer thickness distributions to account for the variation in the matrix interlayer at the ply-ply interface. In this study, we used a single $h(x)$ from the same ten interlayer thickness distributions that yielded a shear stress response closest to the average. Further, the viscosity of the matrix material is required, which we obtained from plate-plate rheometry as will be presented in the next section.

Hence, four parameters are left to be determined for the transient shear flow model: G (Eq. (4)), k_{min}, a, and m (Eq. (10)). These four parameters were estimated by visual inspection of the correlation between model and measurement. A schematic illustration of the effect of the different parameters on the modeled response is shown in Fig. 9. First, the stiffness parameter G was estimated based on the (start-up) slope of the measured friction curves. Secondly, k_{min} was determined based on low sliding rate friction data, at which k_{max} approaches k_{min} and thus both rates were set equal in this step. Next, higher rate friction data were used to determine several k_{max} values at different sliding rates, which were subsequently used to fit a and m according to Eq. (10).

4. Experimental work

The experimental work outlined in this section is part of our previous work [4,5]. For completeness, a brief description will follow in this section, though the reader is kindly referred to Refs. [4,5] for more details.

4.1. Materials

Two unidirectional (UD) carbon fiber-reinforced thermoplastics were investigated, one with a Victrex PEEK 150P matrix and another with a Victrex LM-PAEK AE250P matrix. Both tapes are manufactured by Toray Advanced Composites [62] and are known as Cetex TC1200 (C/PEEK) and TC1225 (C/LM-PAEK), respectively. The fiber volume fraction of both tapes equals approximately 59%. According to the manufacturer, the melting temperature is 343 °C and 305 °C and the advised processing temperature range is 370–400 °C and 340–385 °C for C/PEEK and C/LM-PAEK, respectively.

4.2. Rheometry

The shear viscosity of the neat matrix materials was measured with plate-plate rheometry. Small amplitude oscillatory shear measurements were performed up to 200 rad/s at 380 °C and 390 °C on PEEK and at 365 °C on LM-PAEK material. Using the Cox-Merz rule, the obtained viscosity curves as function of the shear rate were subsequently fit with the Cross model [63]:

$$\eta(\dot{\gamma}) = \frac{\eta_0}{1 + \left(\frac{\eta_0 \dot{\gamma}}{\tau^*}\right)^{(1-n)}}, \tag{11}$$

with η_0 the zero shear viscosity, τ^* the critical shear stress, and n the power law index. The PEEK data was interpolated using an Arrhenius relation on the fitted zero shear viscosity, following the general approach as described by e.g. Osswald and Rudolph [63], to obtain the viscosity curve at 385 °C.

4.3. Ply-ply friction tests

A purpose-built friction tester was used to measure the resistance against slippage between adjacent plies. A detailed description of the setup, which was part of a benchmark exercise [64], can be found in e.g. Refs. [2,15,65]. Specimens were cut from 12-inch wide rolls and each consisted of three 50-mm wide plies: a single central ply measuring 250-mm long and two outer plies measuring 120-mm long with the fibers oriented in the longitudinal direction. The three plies overlapped over a length of 65 mm, resulting in two ply–ply interfaces, and were pressurized between heated platens with contact area A of 50×50 mm^2. After a 5-min heating time, a constant sliding rate V was applied, forcing the central ply to slide against the outer plies. The required pulling force F_{pull} was logged, together with the displacement d and time t. The shear stress per slip interface can then be obtained from:

$$\tau = \frac{F_{pull}}{2A}. \tag{12}$$

Different sliding rates of 5, 25, and 125 mm/min were tested in at least threefold with a fresh specimen for each test. Additionally, single tests were performed at 40 and 60 mm/min to further refine the rate-dependency of the friction response at intermediate rates. The temperature was set at 385 °C and 365 °C for C/PEEK and C/LM-PAEK, respectively, based on the advised processing temperatures. A 15 kPa normal pressure was applied for both materials.

5. Results

The rheometry results will be presented first, followed by the measured ply-ply friction responses of C/PEEK and C/LM-PAEK for different sliding rates, which will be compared with the transient shear flow model.

5.1. Rheometry

The measured viscosity curves of the matrix materials Victrex PEEK 150P and LM-PAEK AE250P are shown in Figs. 7(a) and 7(b), respectively. The PEEK viscosity curves, measured at 380 and 390 °C, were fit with the Cross model (see Eq. (11)). Subsequently, an Arrhenius relation was used to interpolate the zero shear viscosity corresponding to a temperature of 385 °C, as used in the friction experiments. The other Cross model parameters were kept constant and taken equal to the ones obtained from the fit at 380 °C. The result is plotted by the thick black line in Fig. 7(a) and the fit parameters are mentioned in the legend. The measured LM-PAEK viscosity curve, as shown in Fig. 7(b), was also fit with the Cross model (thick black line, see legend for fit parameters). The fit is extrapolated towards shear rates far higher than measured in the plate-plate rheometry experiments to compare

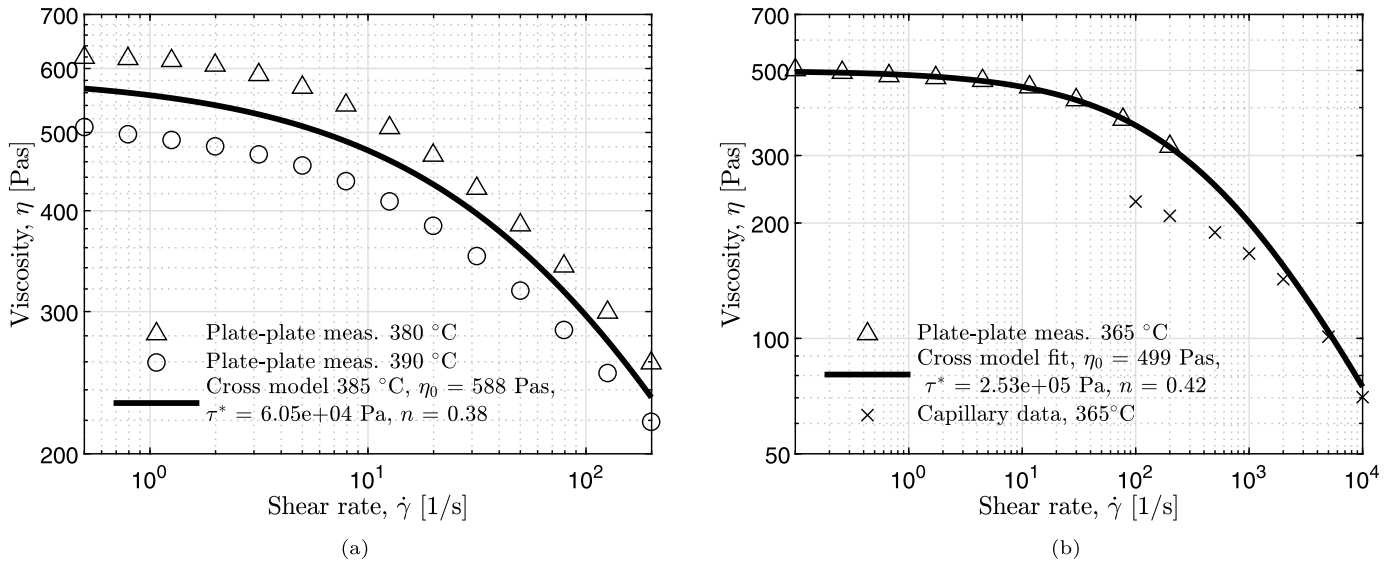

Fig. 7. PEEK 150P viscosity as function of the shear rate measured at 380 and 390 °C (a), which were used to obtain the viscosity curve at 385 °C (thick black line) represented by the Cross model (Eq. (11)) and (b) measured LM-PAEK AE250P viscosity curve at 365 °C with Cross model fit together with viscosity data from the manufacturer Victrex [66] measured with capillary rheometry, interpolated between 360 and 380 °C.
Source: Reproduced from [4].

the fitted viscosity with capillary rheometry data. The capillary data was obtained from interpolation of data measured at 360 and 380 °C, as kindly provided by the manufacturer Victrex plc [66]. Although a discrepancy between model and measurement can be observed at lower shear rates, attributed by the manufacturer to the unreliability of capillary measurements at these low rates, a good correlation is obtained at higher shear rates. Note that these high shear rates are encountered in the friction experiments as well in case of a low matrix interlayer thickness combined with a high sliding rate, e.g. the nominal shear rate equals 2000 s^{-1} for a matrix interlayer thickness of 1 μm with a sliding rate of 125 mm/min.

5.2. Ply-ply friction tests

The ply-ply friction response for different rates is shown in Figs. 8(a) and 8(b) for C/PEEK and C/LM-PAEK, respectively. The average response is plotted for the measurements at 5, 25, and 125 mm/min with the shaded band denoting the standard deviation. The applied sliding rate has a strong effect on the friction response for both materials. The measured friction data at intermediate rates resembles the typical friction response, as schematically illustrated in Fig. 1, exhibiting a peak τ_p and long-time shear stress τ_∞. At higher sliding rates, the peak becomes increasingly sharper with a larger ratio between peak and long-time shear stress, while no peak emerged at the lowest sliding rate measured.

Although the general friction response of both UD tape materials looks similar, small differences can be observed between C/PEEK and C/LM-PAEK (see Fig. 8). The overall friction of C/PEEK is lower compared with C/LM-PAEK when inspecting the peak and long-time shear stresses. Moreover, the C/PEEK friction response exhibits a sharper peak, as seen by the faster shear stress decay compared with the measured response for C/LM-PAEK.

The friction response of the transient shear flow model is plotted for the corresponding sliding rates by the dashed lines in Fig. 8. The transient model correlates well with the measured friction response for both C/PEEK and C/LM-PAEK. The used variables and slip parameters, k_{min}, a, and m, as well as the stiffness parameter G are listed in Table 1.

6. Discussion

The accuracy of the proposed White–Metzner state-rate model in view of the measured friction response for C/PEEK and C/LM-PAEK will be discussed. In particular, the state-rate model used to describe the slip evolution will be addressed. We will relate our modeling efforts with earlier work and propose simplifications to ease implementation in simulation software.

The proposed transient model correlates well with the measured friction response for C/PEEK and C/LM-PAEK, a shown in Fig. 8. The measured and modeled peak and long-time shear stresses are comparable in magnitude and the model accurately accounts for the increase in friction with increasing rate. In general, the measured displacement at the peak correlates well with the model results. Furthermore, the transition in the measured peak response from smooth to sharp with increasing sliding rate is also present in the computed response. At the highest rate, however, the measured peak becomes too sharp for an accurate description with the transient model, while the modeled peak response evolves too rapidly at lower rates.

6.1. Effect of the model parameters

The stress growth at start-up is governed by the stiffness G in the White–Metzner model, dictating the initial slope of the modeled shear stress response. The effect of an increase in G on the modeled response is schematically illustrated in Fig. 9. A steeper slope yields a more rapid stress growth and, therefore, a slightly higher peak shear stress. The determined values for G result in a reasonable correlation between the modeled and measured initial slope. Although we believe that the friction response is dominated by the viscoelastic properties of the matrix material, the measured slope might be affected by slack in the setup as well as tensioning and rearrangements of the fibers in the UD tapes during the measurement.

The rates for the disentanglement (k_d), entanglement (k_e), and conformation (k_c) of surface chains were obtained through linear interpolation between a minimum k_{min} and maximum k_{max} rate (see Eq. (7)), of which the latter depends on the applied sliding rate V according to Eq. (10). The dependency of the rates on V resembles the use of a spectrum of slip relaxation times, as was proposed in other studies [21,30,43], and a faster relaxation through flow-induced disentanglement

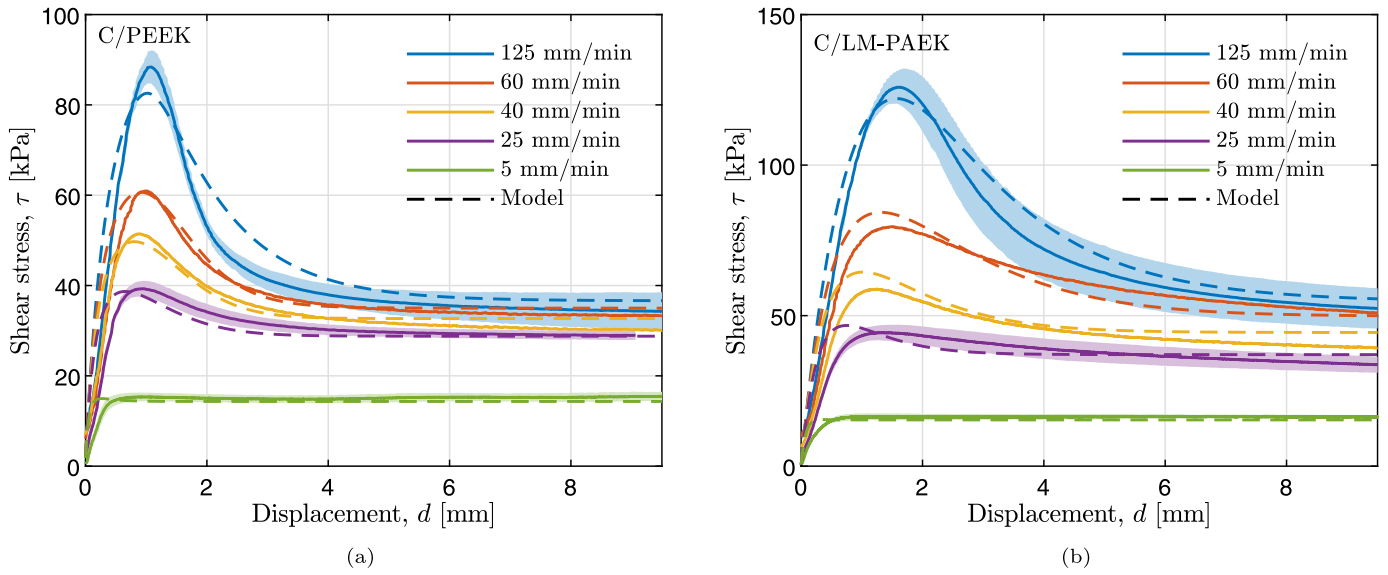

Fig. 8. Ply-ply friction response of (a) C/PEEK and (b) C/LM-PAEK tape for different sliding rates (solid lines) at a temperature of 385 °C and 365 °C, respectively, under a normal pressure of 15 kPa as measured in our earlier work [4]. The shaded bands around the 5, 25, and 125 mm/min friction curves denote the standard deviation. The dashed lines represent the modeled response at the corresponding sliding rates.

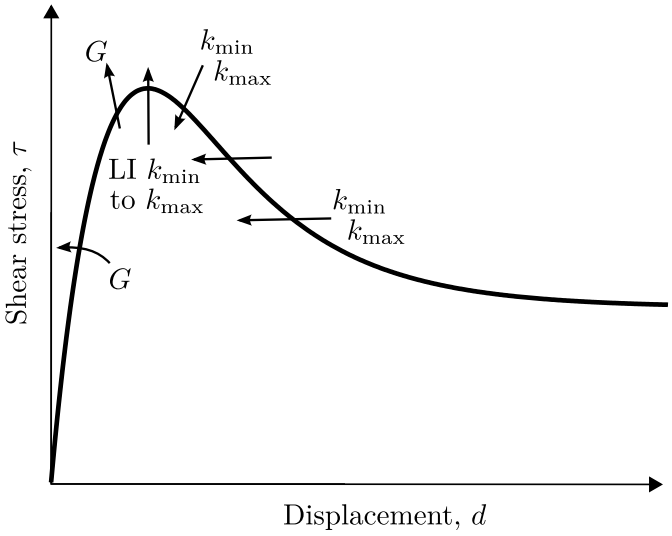

Fig. 9. Schematic illustration of the effect of an increase in G, k_{min}, k_{max}, and the linear interpolation (LI) between a lower k_{min} and higher k_{max} on the modeled response.

by means of mutual sliding of surrounding bulk chains [67,68]. Future work would be to relate the used parameters for the slip evolution to the matrix, the fiber, or the fiber–matrix interfacial properties.

The effect of an increase in k_{min} and k_{max} is included in the schematic model response shown in Fig. 9, indicating that for both rates an increase results in a lower peak response. The linear interpolation (LI) between a lower k_{min} and a higher k_{max} leads to a faster conformation of surface chains to the steady state with evolving slip. Although an overall increase in k_i would result in faster slip evolution as well, the use of a low and high rate leads to more load bearing capacity during start-up, resulting in a higher peak shear stress followed by a more rapid shear stress decay, i.e. a sharper peak. This mechanism resembles the elastic deformation of a temporary network structure followed by breakdown as mentioned in Refs. [22,33,38]. At even higher rates, a more destructive mechanism of forced disentanglement through chain pull-out or breakage might become dominant, which is not accounted for in the proposed model. The lack of such a mechanism might explain why the model is not able to accurately describe the sharp peak measured at the highest rate. Another description for the rates k_i, e.g. using nonlinear interpolation and distinct formulations for k_d and k_c, could also improve the accuracy of the model.

The slip evolution also depends on the local matrix interlayer thickness h at the ply-ply interface. The evolution of the normalized slip velocity V_s/V with time for different h is visualized in Fig. 10(a). The slip velocity increases faster and reaches closer towards the theoretical limit of 0.5 for lower matrix interlayer thicknesses. The slip evolution exhibits an S-shaped curve for all considered thicknesses. This S-shape resembles the response as obtained with Hatzikiriakos' approach [29] using a differential slip equation as shown by Grzelka et al. [45].

A distribution of matrix interlayer thicknesses $h(x)$, as present at the ply-ply interface, is used in the transient model instead of a single, constant thickness. The modeled shear stress is, therefore, a combination of the responses for a wide range of thicknesses for each sliding rate. As mentioned, we used one of the ten matrix interlayer thickness distributions from our earlier work [4] that resulted in an average response. The effect of $h(x)$ on the modeled response is shown in Fig. 10(b), where the thick black line denotes the response for the default $h(x)$ and the blue band represents the lower and upper bound when using the other nine distributions as generated in our earlier work [4].

6.2. Towards implementation in simulation software

The state-rate model can be simplified by using constant and equal rates ($k_{max} = k_{min} = c$), for which the modeled shear stress response is shown in Fig. 11 together with the measured C/PEEK friction data. The correlation between model and measurement reduces, especially at higher rates where the sharp peak is not accurately described. However, the state-rate model gains in simplicity and the system of coupled differential equations of the state-rate model (Eq. (6)) becomes analytically solvable. The analytical solution of the slip velocity is formed by a summation of two exponential functions, resembling the approach of Refs. [55–57].

The use of constant rates is beneficial for implementation in simulation software. Another point in view of numerical implementation is the computation of the shear stress response for each segment in $h(x)$, which is relatively time-consuming. The computational time could be reduced by approximating $h(x)$ by larger segments, as visualized in

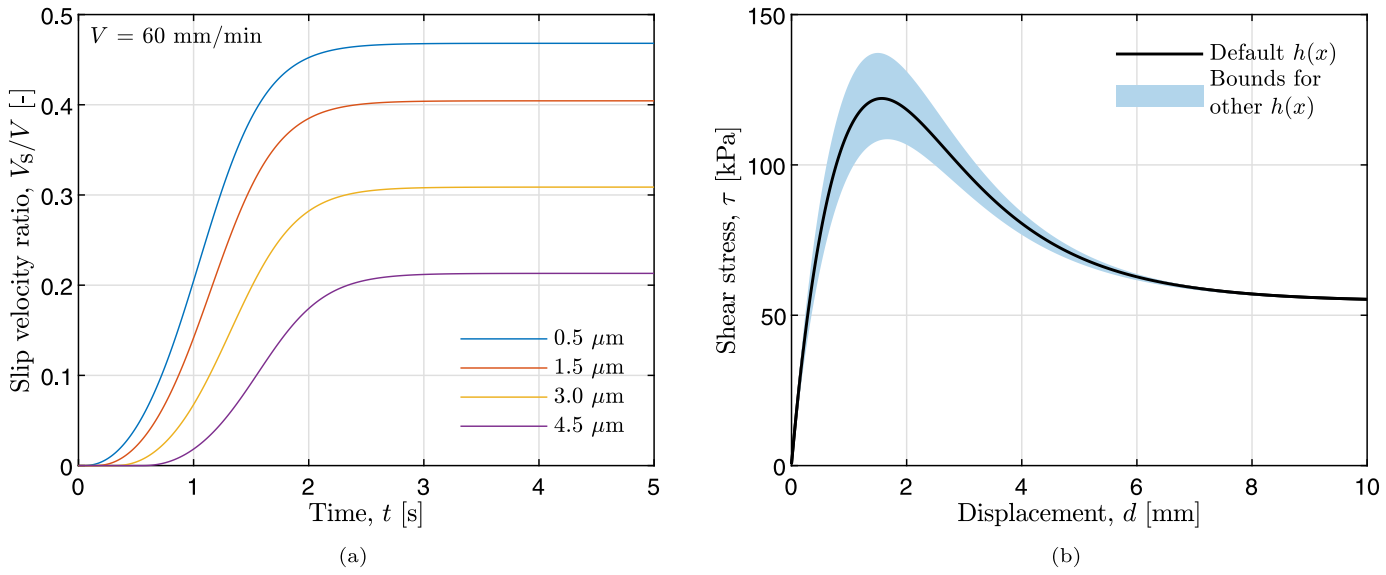

Fig. 10. Effect of the matrix interlayer thickness on (a) the evolution of the normalized slip velocity V_s/V with time and (b) on the modeled response using different matrix interlayer thickness distributions. The thick line represents the response for the default $h(x)$, while the blue band denotes the lower and upper limit of the modeled response for the other nine distributions from our earlier work [4].

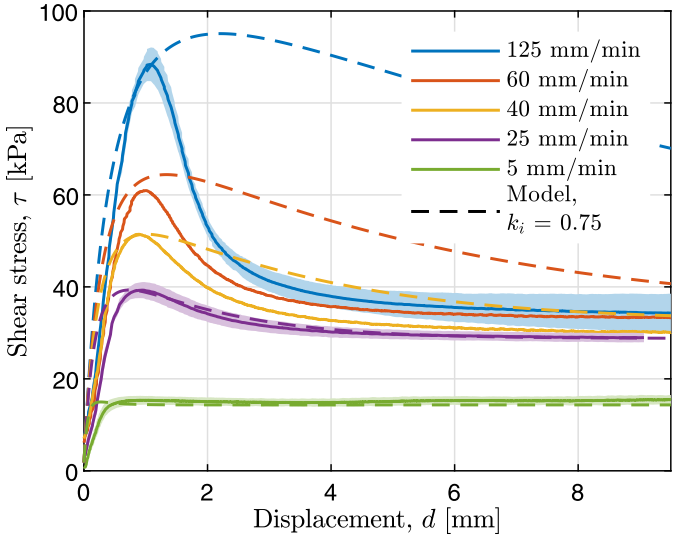

Fig. 11. Measured friction response of C/PEEK for different sliding rates (solid lines, reproduced from [4]) together with modeled response (dashed lines) when using constant rates $k_i = 0.75$ in the state-rate model.

Fig. 12(a). The default $h(x)$ as used in the model is sorted by height and plotted as function of the normalized width. Sorting of the matrix interlayer is possible as the proposed transient model considers a 1D shear flow in the sliding direction, assuming that interference of flow in the perpendicular direction is negligible. The sorted matrix interlayer curve was approximated by ten equal-width segments, of which each height was calculated by equating the enclosed areas of the segment and the matrix interlayer curve at the width boundaries of the segment. The obtained segments are illustrated by the gray lines in Fig. 12(a). The resulting friction response based on this coarse approximation of $h(x)$ with the same parameters as determined earlier (see Table 1) is visualized in Fig. 12(b) together with the measured C/PEEK friction curves, showing a similar correlation as obtained before. The computed response when using the ten segments is alike to the one obtained with the full $h(x)$ (see Fig. 8(a)), though the number of evaluation points reduced from nearly a thousand to only ten. A more sophisticated approach would be to approximate $h(x)$ by e.g. an exponential fit function and to optimize the points where the shear stress response is computed. Anyhow, a proper approximation of $h(x)$ avoids the calculation of numerous local responses and, with that, allows reduction of the computational time without compromising accuracy.

Future work will be to implement the transient shear flow model in simulation software, for which the simplifications as discussed above could be helpful. Additionally, the transient model needs further elaboration to handle the varying sliding rates that are present in a forming simulation, as this work only considered constant sliding rates. In the end, an improved constitutive friction model, including transient effects, will improve the forming predictions with the ultimate goal to enable first-time-right defect-free manufacturing of TPC parts.

7. Conclusion

The transient ply–ply friction response of aligned carbon-fiber reinforced thermoplastics in melt, as measured in a friction tester, exhibits a peak followed by a steady-state shear stress. This friction response, in particular the peak, strongly depends on the applied sliding rate. We proposed a model to describe this transient friction response by considering the viscoelasticity of the matrix material at the ply–ply interface by means of the White–Metzner model combined with local fiber–matrix slip effects through a state-rate model. This state-rate model represents the average state of the polymer chains adsorbed at the fiber surface, describing the disentanglement from the bulk followed by the settlement of these surface chains in a new equilibrium interfacial state in the stationary regime. Hence, the state-rate model describes the transition near the fiber–matrix interface from an initially entangled polymer network towards an average state with less interactions between surface and bulk chains. We related this disentanglement process to the evolution of the slip velocity near the fiber surface, which reduces the local shear rate experienced by the bulk material. In the end, only three parameters are required to describe the slip evolution. Overall, the combined White–Metzner state-rate model accurately captures the measured friction curves of UD C/PEEK and C/LM-PAEK for different constant sliding rates. The model correctly describes the location of the measured peak, as well as the shape of the peak going from smooth at low rates towards sharp at high rates. However, at the highest sliding rate, the measured response exhibited

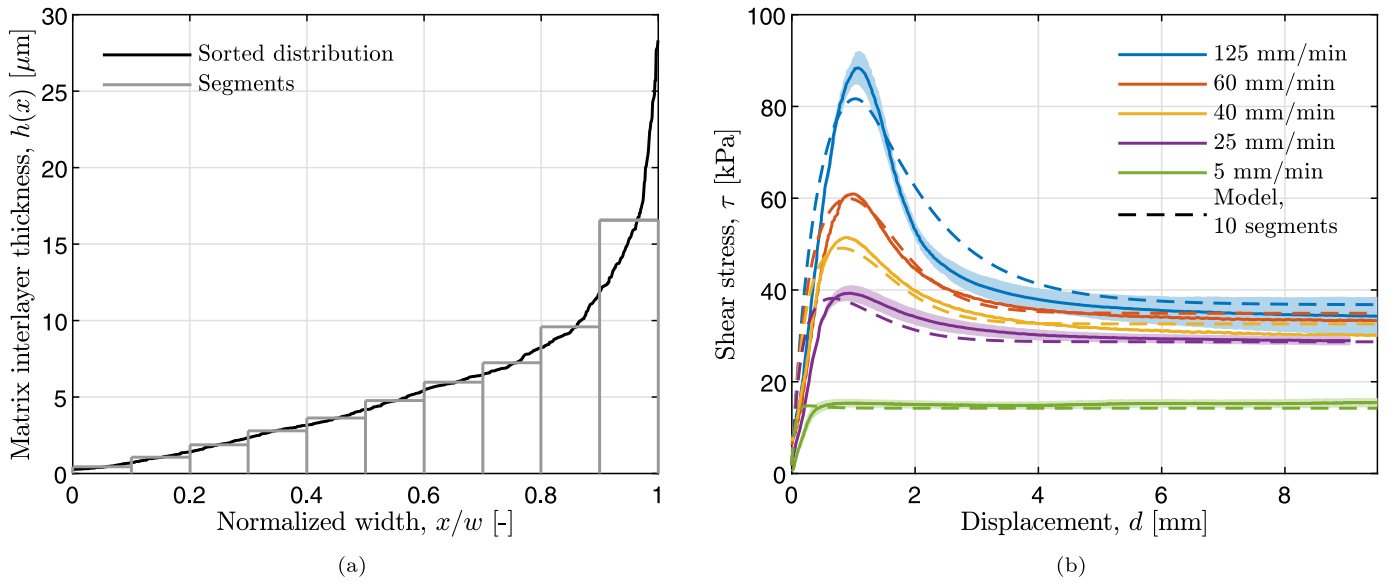

Fig. 12. Sorted matrix interlayer thickness distribution versus the normalized width (black line, reused from [4]) with a coarse approximation by ten segments (gray lines) (a) and (b) C/PEEK friction curves (solid lines, reproduced from [4]) for different sliding rates together with the modeled response (dashed lines) based on the ten segments.

a too sharp peak to describe with the transient shear flow model, while the modeled peak evolves too fast at low sliding rates.

The proposed transient model is promising for the use in forming simulation software considering the good correlation with measurements and its relative simplicity compared to e.g. full molecular dynamics models, though the implementation of this friction model may not be straightforward due to the numerical time integration and the use of a wide matrix interlayer thickness distribution. Simplifications by using constant rates and a coarse approximation of the matrix interlayer thickness distribution reduce the model complexity, without losing too much accuracy.

CRediT authorship contribution statement

E.R. Pierik: Conceptualization, Investigation, Methodology, Software, Validation, Visualization, Writing – original draft. **W.J.B. Grouve:** Conceptualization, Funding acquisition, Project administration, Supervision, Writing – review & editing. **S. Wijskamp:** Resources, Writing – review & editing. **R. Akkerman:** Supervision, Writing – review & editing.

Declaration of competing interest

The authors declare that they have no known competing financial interests or personal relationships that could have appeared to influence the work reported in this paper.

Data availability

The research data will be published in a digital data repository called 4TU.ResearchData, including the measured data, the used scripts and further supplementary data.

Acknowledgments

This work was performed as part of the MaterialenNL research program under project number 17880, which is financed by the Dutch Research Council (NWO). The authors also gratefully acknowledge the financial and technical support from the industrial and academic members of the ThermoPlastic composites Research Center (TPRC). Further, we thank Marten van der Werff for performing the rheometry measurements on PEEK.

References

[1] Long AC. Composites forming technologies. Cambridge, United Kingdom: Woodhead Publishing; 2007.
[2] Sachs U. Friction and bending in thermoplastic composites forming processes (Ph.D. thesis), Enschede, The Netherlands: University of Twente; 2014.
[3] Pierik ER, Grouve WJB, Wijskamp S, Akkerman R. On the origin of start-up effects in ply-ply friction for UD fiber-reinforced thermoplastics in melt. In: 24th international conference on material forming. Liège, Belgium: ESAFORM; 2021, p. 3695.
[4] Pierik ER, Grouve WJB, Wijskamp S, Akkerman R. Prediction of the peak and steady-state ply-ply friction response for UD C/PAEK tapes. Composites A 2022;163:107185.
[5] Pierik ER, Grouve WJB, Wijskamp S, Akkerman R. Modeling the effect of temperature and pressure on the peak and steady-state ply-ply friction response for UD C/PAEK tapes. Composites A 2023;173:107671.
[6] Haanappel SP, Ten Thije RHW, Sachs U, Rietman B, Akkerman R. Formability analyses of uni-directional and textile reinforced thermoplastics. Composites A 2014;56:80–92.
[7] Vanclooster K. Forming of multilayered fabric reinforced thermoplastic composites (Ph.D. thesis), Leuven, Belgium: KU Leuven; 2009.
[8] Murtagh AM, Mallon PJ. Chapter 5 characterisation of shearing and frictional behaviour during sheet forming. In: Bhattacharyya D, editor. In: Composite materials series, vol. 11, Elsevier; 1997, p. 163–216.
[9] Sachs U, Akkerman R. Viscoelastic bending model for continuous fiber-reinforced thermoplastic composites in melt. Composites A 2017;100:333–41.
[10] Pipes RB, Favaloro A, Barocio E, Hicks J. Pure bending of a continuous fiber array suspended in a thermoplastic polymer in melt state. Composites A 2021;149:106561.
[11] Brands D, Wijskamp S, Grouve WJB, Akkerman R. In-plane shear characterization of unidirectional fiber reinforced thermoplastic tape using the bias extension method. Front Mater 2022;9:863952.
[12] Murtagh AM, Monaghan MR, Mallon PJ. Investigation of the interply slip process in continous fibre thermoplastic composites. In: Miravete A, editor. Proceedings of ICCM-9. Madrid, Spain: ICCM; 1993, p. 311–8.
[13] Morris SR, Sun CT. An investigation of interply slip behaviour in AS4/PEEK at forming temperatures. Compos Manuf 1994;5(4):217–24.
[14] Scherer R, Friedrich K. Inter- and intraply-slip flow processes during thermoforming of CF/PP-laminates. Compos Manuf 1991;2(2):92–6.
[15] Ten Thije RHW, Akkerman R. Design of an experimental setup to measure tool-ply and ply-ply friction in thermoplastic laminates. Int J Mater Form 2009;2(1):197–200.
[16] Dörr D, Faisst M, Joppich T, Poppe C, Henning F, Kärger L. Modelling approach for anisotropic inter-ply slippage in finite element forming simulation of thermoplastic UD-tapes. In: 21th international conference on material forming. Palermo, Italy: ESAFORM; 2018, 020005.
[17] Gorczyca-Cole JL, Sherwood JA, Chen J. A friction model for thermostamping commingled glass-polypropylene woven fabrics. Composites A 2007;38(2):393–406.

[18] Ten Thije RHW, Akkerman R, Ubbink M, Van der Meer L. A lubrication approach to friction in thermoplastic composites forming processes. Composites A 2011;42(8):950–60.
[19] Advani SG, Creasy TS, Shuler SF. Chapter 8 rheology of long fiber-reinforced composites in sheet forming. In: Bhattacharyya D, editor. In: Composite materials series, vol. 11, Elsevier; 1997, p. 323–69.
[20] Rietman B, Sachs U, Haanappel SP, Akkerman R. Complex stamp forming of advanced thermoplastic composites. In: 3rd thematic conference on mechanical response of composites. Hannover, Germany: ECCOMAS; 2011, p. 27–34.
[21] Hatzikiriakos SG. Wall slip of molten polymers. Prog Polym Sci 2012;37(4):624–43.
[22] Wang SQ. Nonlinear polymer rheology. Hoboken (NJ), United States of America: John Wiley & Sons; 2017.
[23] Boukany PE, Tapadia P, Wang SQ. Interfacial stick-slip transition in simple shear of entangled melts. J Rheol 2006;50(5):641–54.
[24] Park HE, Lim ST, Smillo F, Dealy JM. Wall slip and spurt flow of polybutadiene. J Rheol 2008;52(2):1201–39.
[25] Fetfatsidis KA, Jauffrès D, Sherwood JA, Chen J. Characterization of the tool/fabric and fabric/fabric friction for woven-fabric composites during the thermostamping process. Int J Mater Form 2013;6(2):209–21.
[26] Chen Q, Boisse P, Park CH, Saouab A, Bréard J. Intra/inter-ply shear behaviors of continuous fiber reinforced thermoplastic composites in thermoforming processes. Compos Struct 2011;93(7):1692–703.
[27] Kapshammer A, Laresser D, Miron MC, Baudach F, Major Z. Characterization and modeling of ply/tool and ply/ply slippage phenomena of unidirectional polycarbonate CF tapes. Polymers 2023;15:3520.
[28] White JL, Metzner AB. Development of constitutive equations for polymeric melts and solutions. J Appl Polym Sci 1963;7:1867–89.
[29] Hatzikiriakos SG, Dealy JM. Wall slip of molten high density polyethylene. I. Sliding plate rheometer studies. J Rheol 1991;35(4):497–523.
[30] Kazatchkov IB, Hatzikiriakos SG. Relaxation effects of slip in shear flow of linear molten polymers. Rheol Acta 2010;49(2010):267–74.
[31] Xu J, Costeux S, Dealy JM, De Decker MN. Use of a sliding plate rheometer to measure the first normal stress difference at high shear rates. Rheol Acta 2007;46(2007):815–24.
[32] Mhetar V, Archer LA. Slip in entangled polymer melts. 2. Effect of surface treatment. Macromolecules 1998;31(24):8617–22.
[33] Boukany PE, Wang SQ. Exploring origins of interfacial yielding and wall slip in entangled linear melts during shear or after shear cessation. Macromolecules 2009;42(6):2222–8.
[34] Hatzikiriakos SG. Appropriate boundary conditions in the flow of molten polymers. Int Polym Process 2009;25:55–62.
[35] Brochard F, de Gennes PG. Shear-dependent slippage at a polymer/solid surface. Langmuir 1992;8(12):3033–7.
[36] Mhetar V, Archer LA. Slip in entangled polymer melts. 1. General features. Macromolecules 1998;31(24):8607–16.
[37] Bergem N. Visualization studies of polymer melt flow anomalies in extrusion. In: C. Klason JK, editor. Proceedings of 7th international congress on rheology. Gothenburg, Sweden: Swedish Society of Rheology; 1976, p. 50–4.
[38] Léger L, Hervet H, Charitat T, Koutsos V. The stick-slip transition in highly entangled poly(styrene-butadiene) melts. Adv Colloid Interface Sci 2001;94:39–52.
[39] Adjari A, Brochard-Wyart F, de Gennes PG, Leibler L, Viovy JL, Rubinstein M. Slippage of an entangled polymer melt on a grafted surface. Physica A 2014;204:17–39.
[40] Maxwell B, Nguyen M. Measurement of the elastic properties of polymer melts. Polym Eng Sci 1979;19(16):1140–50.
[41] Wang SQ. From wall slip to bulk shear banding in entangled polymer solutions. Macromol Chem Phys 2019;220:1800327.
[42] Ebrahimi M, Konaganti VK, Hatzikiriakos SG. Dynamic slip of polydisperse linear polymers using partitioned plate. Phys Fluids 2018;30:030601.
[43] Kazatchkov IB, Hatzikiriakos SG. Dynamic interfacial behavior of linear polymers. In: Aït-Kadi A, Dealy JM, D. F. James MCW, editors. Proceedings of 12th international congress on rheology. Quebec City, Canada: Canadian Rheology Group; 1996, p. 105–6.
[44] Kouallas G, Georgiou GC. Start-up and cessation Newtonian poiseuille and couette flows with dynamic wall slip. Meccanica 2015;50(7):1747–60.
[45] Grzelka M, Antoniuk I, Drockenmuller E, Chennevière A, Léger L. Viscoelasticity-induced onset of slip at the wall for polymer fluids. ACS Macro Lett 2020;9:924–8.
[46] Hatzikiriakos SG, Dealy JM. Role of slip and fracture in the oscillating flow of HDPE in a capillary. J Rheol 1992;36:845–84.
[47] Hatzikiriakos SG, Kalogerakis N. A dynamic slip velocity model for molten polymers based on a network kinetic theory. Rheol Acta 1994;33:38–47.
[48] Hatzikiriakos SG. A brownian dynamics simulation of a polymer/wall interface under shear. Int J Polym Anal Charact 1995;1:87–97.
[49] Dubbeldam JLA, Molenaar J. Self-consistent dynamics of wall slip. Phys Rev E 2003;67:011803.
[50] Stepanyan R, Slot JJM, Molenaar J, Tchesnokov MA. A simple constitutive model for a polymer flow near a polymer-grafted wall. J Rheol 2005;49:1129–51.
[51] Tchesnokov MA, Molenaar J, Slot JJM, Stepanyan R. A molecular model for cohesive slip at polymer melt/solid interfaces. J Chem Phys 2005;122:214711.
[52] Kirk J, Kröger M, Ilg P. Surface disentanglement and slip in a polymer melt: a molecular dynamics study. Macromolecules 2018;51:8996–9010.
[53] Black WB, Graham MD. Wall-slip and polymer-melt flow instability. Phys Rev Lett 1996;77:956–9.
[54] Lan SK, Giacomin AJ, Ding F. Dynamic slip and nonlinear viscoelasticity. Polym Eng Sci 2000;40:507–24.
[55] Joshi YM, Lele KA, Mashelkar RA. Slipping fluids: a unified transient network model. J Non-Newton Fluid Mech 2000;89:303–35.
[56] Ahn KH, Osaki K. A network model for predicting the shear thickening behavior of a poly(vinyl alcohol)-sodium borate aqueous solution. J Non-Newton Fluid Mech 1994;55:215–27.
[57] Lau HC, Schowalter WR. A model for adhesive failure of viscoelastic fluids during flow. J Rheol 1986;30:193–206.
[58] Tseng HC. A revisitation of White–Metzner viscoelastic fluids. Phys Fluids 2021;33:057115.
[59] Macosko CW. Rheology: principles, measurements, and applications. Weinheim, Germany: Wiley-VCH; 1994.
[60] Cogswell FN. Thermoplastic aromatic polymer composites. Oxford, United Kingdom: Butterworth-Heinemann; 1992.
[61] Deignan A, Stanley WF, McCarthy MA. Insights into wide variations in carbon fibre/polyetheretherketone rheology data under automated tape placement processing conditions. J Compos Mater 2017;52(16):2213–28.
[62] Toray Advanced Composites. Innovation by chemistry. 2022, URL https://www.toraytac.com/.
[63] Osswald T, Rudolph N. Polymer rheology. München, Germany: Carl Hanser Verlag.
[64] Sachs U, Akkerman R, Fetfatsidis K, Vidal-Sallé E, Schumacher J, Ziegmann G, Allaoui S, Hivet G, Maron B, Vanclooster K, Lomov SV. Characterization of the dynamic friction of woven fabrics: experimental methods and benchmark results. Composites A 2014;67:289–98.
[65] Akkerman R, Ten Thije RHW, Sachs U, De Rooij M. Friction in textile thermoplastic composites forming. In: Recent advances in textile composites. Lille, France: TEXCOMP; 2010, p. 271–9.
[66] Victrex plc. Shaping future performance. 2022, URL https://www.victrex.com/.
[67] Ianniruberto G, Marrucci G. On compatibility of the Cox-Merz rule with the model of Doi and Edwards. J Non-Newton Fluid Mech 1996;65:241–6.
[68] Marrucci G. Dynamics of entanglements: a nonlinear model consistent with the Cox-Merz rule. J Non-Newton Fluid Mech 1996;62:279–89.